

# SnareNet: Flexible Repair Layers for Neural Networks with Hard Constraints

Ya-Chi Chu\*

Alkiviades Boukas†

Madeleine Udell‡

February 11, 2026

## Abstract

Neural networks are increasingly used as surrogate solvers and control policies, but unconstrained predictions can violate physical, operational, or safety requirements. We propose SnareNet, a feasibility-controlled architecture for learning mappings whose outputs must satisfy input-dependent nonlinear constraints. SnareNet appends a differentiable repair layer that navigates in the constraint map’s range space, steering iterates toward feasibility and producing a repaired output that satisfies constraints to a user-specified tolerance. To stabilize end-to-end training, we introduce *adaptive relaxation*, which designs a relaxed feasible set that snares the neural network at initialization and shrinks it into the feasible set, enabling early exploration and strict feasibility later in training. On optimization-learning and trajectory planning benchmarks, SnareNet consistently attains improved objective quality while satisfying constraints more reliably than prior work.

## 1 Introduction

Deep learning (DL) models have emerged as powerful tools across diverse applications, from computational biology [18, 4] and drug discovery [13, 39] to robotics [23] and autonomous systems [14]. Their success stems from an ability to learn complex patterns from data and make accurate predictions in high-dimensional spaces. Increasingly, neural networks (NNs) are being deployed as fast surrogate models that can replace or supplement traditional computational methods. For instance, in domains where the same type of problem must be solved frequently under real-time constraints—such as power systems operation [31] and robotic control [38]—or where individual solutions require expensive computation—such as weather forecasting [22, 6] and fluid dynamics simulations [21]—NNs offer orders-of-magnitude speedups compared to conventional solvers while maintaining competitive accuracy.

Despite versatility of DL models, standard DL architectures deliver unconstrained outputs. While simple constraints like simplex constraints and coordinate-wise bounds can be readily enforced through architecture design, it is challenging to enforce complex constraints, even for linear constraints. Research on *constrained neural networks* is growing in the past few years [3, 27, 17], driven by several compelling needs.

First, many critical applications require constrained outputs to ensure validity and safety. In learning-based control policies, outputs must satisfy safety constraints and physical actuator limits to prevent catastrophic failures [1]. In protein structure prediction, generated structures must obey fundamental physical constraints such as proper bond geometries, tetrahedral atomic chirality,

---

\*Department of Mathematics, Stanford University, CA, United States; email: ycchu97@stanford.edu

†Institute for Computational and Mathematical Engineering, Stanford University, CA, United States; email: aboukas@stanford.edu

‡Department of Management Science and Engineering, Stanford University, CA, United States; email: udell@stanford.edu

and the absence of steric clashes to represent physically valid molecular conformations [8]. In applications such as optimal power flow in electrical grids or resource allocation in supply chains, outputs must satisfy operational constraints including power balance equations, capacity limits, and other problem-specific requirements that define an executable solution. Violating these constraints can lead to solutions that are not only suboptimal but potentially dangerous or nonsensical in practice.

Secondly, constraints provide a mechanism to inject domain knowledge and inductive biases into NNs, which can potentially improve generalization, particularly when training data is limited. In physics-informed neural networks [33], enforcing boundary conditions and physical laws as constraints guides the learning process toward more accurate solutions [25]. By encoding known structural properties of the problem into the network architecture, we guide the learning process toward physically plausible or operationally valid solutions.

The earliest and straightforward approach to handle constraints in NNs adds constraint violations as penalty terms in the loss function [32, 41, 29], known as *soft constraint* approaches. However, this approach provides no guarantees on constraint satisfaction at inference time. Typical gradient-based training with soft constraints produces constraint violations on the order of  $10^{-2}$  or worse [10], leading to physically nonsensical or operationally infeasible solutions. Perhaps more surprisingly, our numerical experiments reveal that soft constraint training can be counterproductive even as a warm-start strategy. These observations underscore the necessity for hard constraint enforcement mechanisms that provide both feasibility and efficient training.

In this paper, we introduce SnareNet (Figure 1), a novel framework to enforce nonlinear, input-dependent constraints on NNs while preserving their approximation capabilities and enabling end-to-end training. Our key contributions are:

- *A practical framework:* We propose SnareNet, which can enforce nonlinear, input-dependent constraints on neural network outputs.
- *Adaptive relaxation training paradigm:* We introduce a novel training strategy that progressively tightens constraint satisfaction during training, balancing feasibility and optimality while avoiding the pathological behaviors often observed in projection-based methods.
- *Feasibility control:* SnareNet enables practitioners to explicitly control the desired level of constraint satisfaction, allowing for application-specific trade-offs between strict feasibility and solution quality.
- *Broad applicability:* We demonstrate SnareNet’s effectiveness on two problem classes, optimization learning tasks and neural control policies. SnareNet consistently produces feasible solutions with better objective values compared to state-of-the-art baselines.

The remainder of this paper is organized as follows. Section 2 introduces the problem of constrained NN learning and review the literature. Section 3 motivates SnareNet from linear constraints. Section 4 presents our SnareNet for nonlinear constraints and our adaptive relaxation training paradigm. Section 5 demonstrates our experiments on SnareNet. Section 6 concludes with a discussion of future directions. We interleave related literature review into Section 2 and Section 4 since literature were integral to the development of SnareNet. For a dedicated related literature section, please see Appendix A.

## 2 Constrained Neural Networks

The fundamental task in deep learning applications is to learn complex input-output mappings  $\Phi : \mathcal{X} \rightarrow \mathcal{Y}$  from data. Given input  $x \in \mathcal{X}$ , the deep learning model  $\mathcal{M}_\theta : \mathcal{X} \rightarrow \mathcal{Y}$  parametrized by weights  $\theta$  is expected to produce an output  $\hat{y} = \mathcal{M}_\theta(x)$  that approximates  $y = \Phi(x)$ .

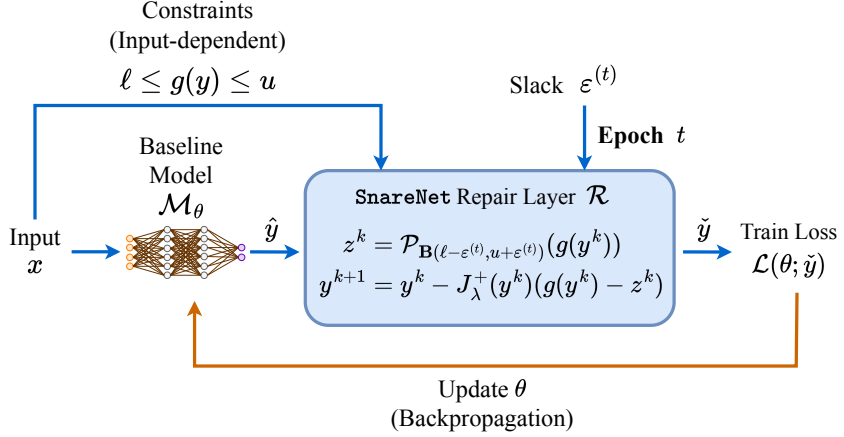


Figure 1: Architecture design of SnareNet.

These deep learning models are typically trained by minimizing an empirical risk over a finite training dataset  $\mathcal{X}_{\text{train}} \subset \mathcal{X}$  defined by  $\mathcal{L}(\theta) = \frac{1}{|\mathcal{X}_{\text{train}}|} \sum_{x \in \mathcal{X}_{\text{train}}} \ell(\theta; x)$ , where  $\ell(\theta; x)$  denotes a suitable loss function measuring the discrepancy between predictions and targets for input  $x$  under model parameter  $\theta$ . For simplicity, we consider the setting where  $\mathcal{X} \subset \mathbb{R}^d$  and  $\mathcal{Y} \subset \mathbb{R}^n$  admit vector representations.

In this paper, we consider the task to impose input-dependent (i.e.,  $x$ -dependent) constraints on the output  $y$ , which take the form:

$$\ell_x \leq g_x(y) \leq u_x, \quad (\text{abbrev. } \ell \leq g(y) \leq u) \quad (1)$$

where  $g : \mathbb{R}^n \rightarrow \mathbb{R}^m$  is differentiable,  $\ell, u \in (\mathbb{R} \cup \{\pm\infty\})^m$  are lower and upper bounds respectively, and all  $g, \ell, u$  are parametrized by input  $x$ . For notational simplicity, we suppress the dependence of  $g, \ell, u$  on  $x$  throughout the paper. The formulation in (1) encompasses equality constraints when  $\ell_i = u_i$  for index  $i$ , as well as one-sided constraints when  $\ell_i = -\infty$  or  $u_i = \infty$ . Throughout the paper, we assume the feasible set  $\mathcal{C} := \{y \in \mathcal{Y} \mid \ell \leq g(y) \leq u\}$  is non-empty for any  $x \in \mathcal{X}$  of interest.

## 2.1 Soft-Constraint Methods

To encourage the model  $\mathcal{M}_\theta$  to produce feasible outputs, early approaches augment the loss function with penalty terms that discourage constraint violations by the output<sup>1</sup>  $\hat{y} = \hat{y}(\theta, x) := \mathcal{M}_\theta(x)$ , also called a *soft loss*:

$$\ell_{\text{soft}}(\theta; x) = \ell(\theta; x) + \mu_u \|\text{ReLU}(g(\hat{y}) - u)\|^2 + \mu_\ell \|\text{ReLU}(\ell - g(\hat{y}))\|^2, \quad (2)$$

where  $\mu_u > 0$  and  $\mu_\ell > 0$  are penalty weights that determine the strength of the penalty, and  $\text{ReLU}(\cdot) := \max(0, \cdot)$  is applied elementwise. The soft loss allows the use of standard unconstrained optimization techniques during training. This soft constraint methodology is commonly used for data-parameterized constrained optimization problems [37] and for solving partial differential equations [33, 9]. While penalty methods are straightforward to implement and broadly applicable, models trained with soft loss generally violate constraints on unseen problem instances. Strict constraint satisfaction requires setting  $\mu_u$  and  $\mu_\ell$  to infinity (or a very large number), which however makes the soft loss infinitely ill-conditioned and hard to solve [34].

<sup>1</sup>We denote the output by  $\hat{y}$  for simplicity when the dependence on  $\theta$  and  $x$  is clear from the context.

## 2.2 Hard-Constraint Methods

To impose the constraints (1) on the output of a baseline model  $\mathcal{M}_\theta$ , a more sophisticated approach appends a *repair module*<sup>2</sup>  $\mathcal{R} : \mathbb{R}^n \rightarrow \mathbb{R}^n$  that maps any potentially infeasible output  $\hat{y}$  to a feasible one  $\check{y}$ . We use  $\hat{y} = \mathcal{M}_\theta(x)$ , pronounced “y-hat”, to denote the approximate solution from the baseline model, which is potentially infeasible; and we use  $\check{y} = \mathcal{R}(\hat{y})$ , pronounced “y-check”, to denote the solution after applying the repair module, which is enforced to be feasible. Two paradigms have appeared in the literature to couple repair modules to a baseline neural net, post-processing and end-to-end training.

**Post-Processing for Feasibility.** The post-processing approach applies the repair module only during inference, but does not allow differentiable training for model parameters  $\theta$ . The simplest post-processing approach is projection onto the feasible set. Given any test instance  $x_{\text{test}}$  and a trained model  $\mathcal{M}_\theta$ , the repair module projects the baseline output onto the feasible set, i.e.,

$$\mathcal{R}(\hat{y}) := \arg \min_{y \in \mathcal{C}} \|y - \mathcal{M}_\theta(x_{\text{test}})\|^2. \quad (3)$$

When  $\mathcal{C}$  is convex, problem (3) is a convex program that typically can be reliably solved by existing optimization solvers. When  $\mathcal{C}$  is non-convex, optimization solvers still reliably find feasible (but not always optimal) solutions to Equation (3). Alternatively, Liang et al. [26] propose to use an auxiliary deep learning model that learns a homeomorphic mapping from the feasible set to the unit ball. However, to project an infeasible solution  $\hat{y}$  to the feasible set, they require binary search, which precludes end-to-end training of the combined system.

The post-processing approach can lead to several critical problems as demonstrated in Grontas et al. [15, Appendix C.4]: models trained without active constraints may diverge on unbounded objectives. Even when they converge, solution quality may be poor after projection since the baseline model fails to anticipate the repair operation.

**Trainable Layers for Feasibility.** On the other hand, the end-to-end approach activates the repair layer during both training and inference, allowing gradients of model weights  $\theta$  to flow through the repair operation. The baseline model  $\mathcal{M}_\theta$  can therefore adapt to the repair operation. To enable gradient-based optimization of the model parameters  $\theta$  via backpropagation, the repair layer must use only operations that are differentiable almost everywhere. State-of-the-art trainable repair layers typically employ a fixed number of iterative updates derived from classical optimization algorithms, such as DC3 [10] and II net [15]. DC3 predicts an initial solution using a soft penalty formulation and moves it toward the feasible region via equality completion and gradient descent on the distance to feasibility. II net decomposes an affine feasible set as the intersection of two higher-dimensional convex sets and applies Douglas-Rachford algorithm to find a feasible solution, in which the computational efficiency is improved by restricting the framework to linear and box constraints. While these iterative approaches improve constraint satisfaction on test instances compared to the baseline model  $\mathcal{M}_\theta$ , backpropagating through these iterations requires intensive GPU memory. In contrast, HardNet [28] uses a closed-form repair layer that guarantees exact feasibility up to machine precision and enables efficient backpropagation. However, HardNet is limited to linear constraints and often produces suboptimal solutions.

## 3 Motivation from Linear Constraints

SnareNet is trained end-to-end through a differentiable repair layer (see Figure 1). For simplicity, this section motivates SnareNet in the special case of linear constraints.

---

<sup>2</sup>We borrow the word “repair” from the term *repair layer* in Van Hentenryck [37], but we call  $\mathcal{R}$  a *layer* only if it is trainable. The same concept has also been referred to as a *projection layer* [28, 15, 26] or a *feasibility layer* [24, 30] in the literature when the repair module is trainable.

### 3.1 Closed-Form Repair Layer for Linear Constraints

HardNet [28] demonstrated that iterative repair layers are unnecessary by introducing a closed-form repair layer that strictly enforces all linear constraints  $\ell \leq Ay \leq u$  when  $A \in \mathbb{R}^{m \times n}$  has full row rank:

$$\mathcal{R}(\hat{y}) := \hat{y} + A^+ \boldsymbol{\delta}(A\hat{y}; \ell, u), \quad \text{where } \boldsymbol{\delta}(z; \ell, u) := \text{ReLU}(\ell - z) - \text{ReLU}(z - u) \quad (4)$$

and  $A^+$  is the pseudoinverse of  $A$ . We call  $\boldsymbol{\delta}(z; \ell, u) \in \mathbb{R}^m$  the *correction vector* to the box  $\mathbf{B}(\ell, u) := \{z \in \mathbb{R}^m \mid \ell_i \leq z_i \leq u_i, \forall i \in [m]\}$ , since

$$\mathcal{P}_{\mathbf{B}(\ell, u)}(z) := \begin{cases} z_i, & \text{if } \ell_i \leq z_i \leq u_i; \\ \ell_i, & \text{if } z_i \leq \ell_i; \\ u_i, & \text{if } z_i \geq u_i; \end{cases} = z + \boldsymbol{\delta}(z; \ell, u).$$

That is,  $\boldsymbol{\delta}(z; \ell, u)$  corrects the vector  $z$  to the box  $\mathbf{B}(\ell, u)$  by elementwise projection. Min and Azizan [28, Theorem 2] shows that if  $A$  has full row rank, then the repair layer (4) strictly enforces linear feasibility: for each constraint  $i$  (row  $a_i$  of  $A$ ), the repaired output satisfies

$$a_i^\top \mathcal{R}(\hat{y}) = \begin{cases} \ell_i, & \text{if } a_i^\top \hat{y} < \ell_i; \\ u_i, & \text{if } a_i^\top \hat{y} > u_i; \\ a_i^\top \hat{y}, & \text{if } \ell_i \leq a_i^\top \hat{y} \leq u_i. \end{cases} \quad (5)$$

### 3.2 Preimage Perspective

Building on HardNet, we observe that the feasible set  $\mathcal{C}$  can be expressed as the preimage of  $\mathbf{B}(\ell, u)$  under the map  $A$ :

$$\begin{aligned} \mathcal{C} &:= \{y \in \mathbb{R}^n \mid \ell \leq Ay \leq u\} \\ &= \{y \in \mathbb{R}^n \mid Ay \in \mathbf{B}(\ell, u)\} \\ &= \text{Preimage of } \mathbf{B}(\ell, u) \text{ under } A. \end{aligned}$$

HardNet chooses a particular feasible solution  $\tilde{y} = \mathcal{R}(\hat{y})$  that lies in the preimage of the special point  $\mathcal{P}_{\mathbf{B}(\ell, u)}(A\hat{y})$ . When  $A$  has full row rank (i.e.,  $A$  is surjective), every vector  $z$  admits a non-empty preimage. In particular,  $A^+z$  given by the pseudoinverse always lies in the preimage of  $z$ .

In this interpretation, the HardNet update 1) decomposes

$$\mathcal{P}_{\mathbf{B}(\ell, u)}(A\hat{y}) = A\hat{y} + \boldsymbol{\delta}(A\hat{y}; \ell, u);$$

and then 2) adjusts  $\hat{y}$  by the vector  $A^+ \boldsymbol{\delta}(A\hat{y}; \ell, u)$ , which lies in the preimage of the correction vector. The linearity of  $A$  ensures  $A^+ \boldsymbol{\delta}(A\hat{y}; \ell, u)$  serves as a feasibility correction:

$$A(\hat{y} + A^+ \boldsymbol{\delta}(A\hat{y}; \ell, u)) = A\hat{y} + \boldsymbol{\delta}(A\hat{y}; \ell, u) = \mathcal{P}_{\mathbf{B}(\ell, u)}(A\hat{y}).$$

### 3.3 Challenges From Linear to Non-Linear

HardNet's particular choice of  $\tilde{y}$  does not directly extend to nonlinear constraints. Example 1 illustrates the challenge:

*Example 1.* Constrain  $y \in \mathbb{R}^2$  to the intersection of two disks of radius  $3/2$ , centered at  $(-1, 0)$  and  $(1, 0)$ :

$$g(y) = \begin{bmatrix} g_1(y) \\ g_2(y) \end{bmatrix} := \begin{bmatrix} (y_1 + 1)^2 + y_2^2 \\ (y_1 - 1)^2 + y_2^2 \end{bmatrix} \leq u := \begin{bmatrix} 9/4 \\ 9/4 \end{bmatrix}.$$

$$y \in \mathbb{R}^n \quad z = g(y) \in \mathbb{R}^m$$

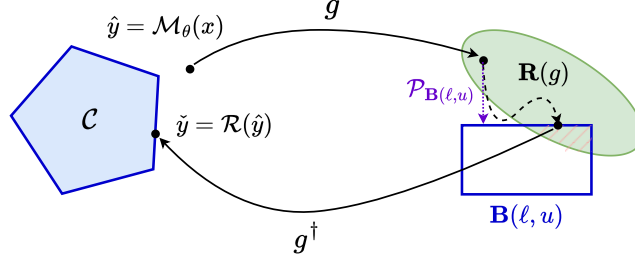


Figure 2: The infeasible point  $\hat{y} = \mathcal{M}_\theta(x)$  is mapped to an image point  $g(\hat{y}) \in \mathbb{R}^m$  that lies outside the box  $\mathbf{B}(\ell, u)$ . The box projection  $\mathcal{P}_{\mathbf{B}(\ell, u)}(g(\hat{y}))$  might have no preimage under non-linear  $g$  since it might not lie in joint numerical range  $\mathbf{R}(g)$ . SnareNet finds a path to approach an image point in the intersection  $\mathbf{R}(g) \cap \mathbf{B}(\ell, u)$ , the preimage of which will be feasible.

Now, consider the infeasible prediction  $\hat{y} = (-1, 0)$ , which violates the second constraints but satisfies the first one as  $g_1(\hat{y}) = 0$  and  $g_2(\hat{y}) = 4$ . The box projection of  $g(\hat{y})$  is  $\mathcal{P}_{(-\infty, u)}(g(\hat{y})) = (0, \frac{9}{4})$ . However, there is *no* point  $y \in \mathbb{R}^2$  such that  $g(y) = (0, \frac{9}{4})$ . That is, the system

$$\begin{cases} g_1(y_1, y_2) = (y_1 + 1)^2 + y_2^2 = 0 \\ g_2(y_1, y_2) = (y_1 - 1)^2 + y_2^2 = \frac{9}{4} \end{cases}$$

has no solution and the preimage of  $(0, \frac{9}{4})$  under  $g$  is empty.

This example reveals the fundamental difficulty: unlike linear mappings, the *joint numerical range*  $\mathbf{R}(g) := \{g(y) \in \mathbb{R}^m \mid y \in \mathbb{R}^n\}$  of a non-linear function  $g$  is typically a proper subset of  $\mathbb{R}^m$ . Consequently, projecting  $g(\hat{y})$  onto the box  $\mathbf{B}(\ell, u)$  may produce a point that has no preimage under  $g$ . To guarantee feasibility, we must instead move towards the intersection  $\mathbf{R}(g) \cap \mathbf{B}(\ell, u)$ , which characterizes points that are both (i) in the range of  $g$  (ensuring a preimage exists) and (ii) within the feasible box (ensuring constraint satisfaction). See Figure 2.

## 4 SnareNet

This section introduces SnareNet, which efficiently finds a feasible point satisfying constraints (1).

### 4.1 Adaptive Newton Update

Given an image point  $z \in \mathbf{R}(g) \cap \mathbf{B}(\ell, u)$ , Newton's method can find a feasible solution  $\check{y} \in \mathcal{C}$  by solving the non-linear system  $g(y) = z$ . SnareNet uses the box projection of  $g(y^k)$  as the initial  $z^k$  at each Newton iteration:

$$\begin{aligned} z^k &= \mathcal{P}_{\mathbf{B}(\ell, u)}(g(y^k)) \\ y^{k+1} &= \arg \min_y \|J_g(y^k)(y - y^k) + g(y^k) - z^k\|^2 \end{aligned} \tag{6}$$

$$= y^k - J_g(y^k)^+(g(y^k) - z^k) \tag{7}$$

where  $J_g(y) \in \mathbb{R}^{m \times n}$  is the Jacobian of  $g$ . When  $g = A$  is linear and  $A$  has full row rank,  $z^k$  must lie in  $\mathbf{R}(A) \cap \mathbf{B}(\ell, u) = \mathbf{B}(\ell, u)$ , so Newton's method converges in one iteration and the update (7) reduces to (4) in HardNet.

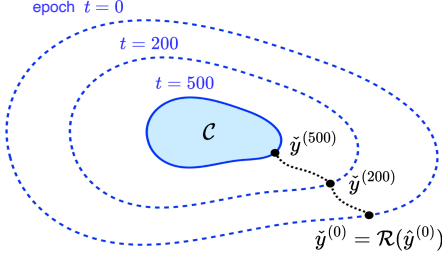


Figure 3: Illustration of adaptive constraints relaxation. The figure illustrates a schedule in which  $\varepsilon^{(t)} = 0$  for  $t \geq 500$ . At epoch  $t$ , the repair layer  $\mathcal{R}$  enforces the output  $\tilde{y}^{(t)}$  lies in the relaxed constraint set  $\mathcal{C}_{\varepsilon^{(t)}} = \{y \in \mathbb{R}^n \mid \ell - \varepsilon^{(t)} \leq g(y) \leq u + \varepsilon^{(t)}\}$ .

## 4.2 Levenberg–Marquardt Regularization

Newton’s method (6) linearizes  $g$  at  $y_k$  and minimizes the residual of the linearized system. The linearization approximates  $g$  only locally, so Newton’s method requires safeguards to ensure convergence. SnareNet uses Levenberg–Marquardt (LM) regularization, replacing (6) by

$$\min_y \|J_g(y^k)(y - y^k) + g(y^k) - z^k\|^2 + \lambda \|y - y^k\|^2. \quad (8)$$

The regularization term  $\lambda \|y - y^k\|^2$  with  $\lambda > 0$  ensures the new point is close to  $y^k$ , at which  $g$  is linearized. The regularized algorithm takes the form

$$y^{k+1} = y^k - J_\lambda^\dagger(y^k)(g(y^k) - z^k), \quad (9)$$

where  $J_\lambda^\dagger(y^k) := [J_g(y^k)^\top J_g(y^k) + \lambda I]^{-1} J_g(y^k)^\top$ . SnareNet terminates when the update magnitude or constraint violation falls below a prescribed tolerance or the iteration limit is reached.

## 4.3 Adaptive Relaxation

Enforcing strict constraints during early-stage training can harm performance. Min and Azizan [28] observes that immediate enforcement prevents models from reaching better-optimized final states, and solves the problem by disabling the repair layer for the first few epochs. These “soft-epochs” instead penalize the constraint in the objective. Nguyen and Donti [30] show that randomly initialized networks produce large violations that force the repair layer to work overtime and reduce the quality of the final solution.

SnareNet instead uses a new *adaptive relaxation* training paradigm that snares the neural network at initialization and shrinks it into the feasible set throughout the training process. Rather than strictly enforcing the constraints  $\ell \leq g(y) \leq u$  from the beginning of training, we repair the approximate solution  $\hat{y}$  towards a relaxed feasible set

$$\mathcal{C}_{\varepsilon^{(t)}} := \{y \in \mathbb{R}^n \mid \ell - \varepsilon^{(t)} \leq g(y) \leq u + \varepsilon^{(t)}\},$$

parametrized by a slack  $\varepsilon^{(t)} \geq 0$  at epoch  $t$ . This slack progressively decreases to zero over the training epochs  $t = 1, 2, \dots, T$ , allowing the model to explore a broader solution space initially while gradually tightening the constraints (see Figure 3). We ensure exact feasibility during the last few training epochs by setting  $\varepsilon^{(t)} = 0$ . SnareNet initializes the slack at epoch  $t = 0$  to ensure the untrained model  $\mathcal{M}_\theta$  satisfies the relaxed constraints, and linearly decays  $\varepsilon^{(t)}$  to zero over a preset decay horizon  $T_d < T$ .

At epoch  $t$ , SnareNet projects the image point  $g(y^k)$  of every LM-iterate  $y^k$  to the relaxed box with slack  $\varepsilon^{(t)}$ :

$$z^k := \mathcal{P}_{\mathbf{B}(\ell - \varepsilon^{(t)}, u + \varepsilon^{(t)})}(g(y^k)) \quad (10)$$

Algorithm 1 provides the pseudocode for this repair layer.

---

**Algorithm 1** Repair layer in SnareNet

---

```

1: assume  $\hat{y} = \mathcal{M}_\theta(x)$  and constraints  $\ell \leq g(y) \leq u$ 
2: function  $\mathcal{R}(\hat{y}, \lambda, \varepsilon)$ 
3:   init  $y^0 = \hat{y}$ 
4:   for  $k = 0, 1, 2, \dots$  until convergence do
5:     compute  $z^k$  using Equation (10) with  $\varepsilon$ 
6:     update  $y^{k+1}$  using Equation (9) with  $\lambda$ 
7:   end for
8:   return  $\check{y} = y^{k+1}$ 
9: end function

```

---

## 5 Experiments

This section demonstrates the effectiveness of SnareNet on optimization learning and neural control policies.<sup>3</sup>

### 5.1 Optimization Learning

The *optimization learning* [37] task seeks a fast surrogate neural solver for a family of optimization problems parametrized by input  $x \in \mathcal{X}$ :

$$\min_{y \in \mathbb{R}^n} f_x(y) \text{ subject to } \ell_x \leq g_x(y) \leq u_x, \quad (11)$$

Both the objective  $f_x : \mathbb{R}^n \rightarrow \mathbb{R}$  and feasible set  $\ell_x \leq g_x(y) \leq u_x$  are parametrized. Problems of the form (11) can be non-linear and non-convex, and can be slow to solve with traditional optimization solvers. The goal of optimization learning is to learn a model  $\mathcal{M}_\theta$  that approximates the solution map  $\Phi : \mathcal{X} \rightarrow \mathbb{R}^n$ , which maps the instance parameter  $x$  to optimal solution  $y^* = \Phi(x)$  of (11). In particular,  $\mathcal{M}_\theta$  must produce a feasible solution for all  $x \in \mathcal{X}$ .

**Families of Problems.** We consider two families of parametric optimization problems, each of which consists of 10000 problem instances and is split into train/valid/test set in the ratio 8:1:1. One family has linear constraints while the other has nonlinear constraints:

1. *Linearly-Constrained Non-Convex Programs (NCPs)*: This family of problems, also considered by Donti et al. [10] and Min and Azizan [28], take the form

$$\begin{aligned} \min_{y \in \mathbb{R}^n} \quad & \frac{1}{2} y^T Q y + p^T \sin(y) \\ \text{s.t.} \quad & A y \leq b, \quad C y = x, \end{aligned}$$

where  $Q \in \mathbb{R}^{n \times n} \succ 0$ ,  $p \in \mathbb{R}^n$ ,  $A \in \mathbb{R}^{n_{\text{ineq}} \times n}$ ,  $C \in \mathbb{R}^{n_{\text{eq}} \times n}$ , and  $b \in \mathbb{R}^{n_{\text{ineq}}}$  are constants, and  $x \in \mathbb{R}^{n_{\text{eq}}}$  is the input.

2. *Quadratically Constrained Quadratic Programs (QCQPs)*: This family of problems minimizes a convex quadratic objective subject to convex quadratic constraints and linear equality constraints:

$$\begin{aligned} \min_{y \in \mathbb{R}^n} \quad & \frac{1}{2} y^T Q y + p^T y \\ \text{s.t.} \quad & y^T H_i y + g_i^T y \leq h_i, \quad i = 1, \dots, n_{\text{ineq}} \\ & C y = x, \end{aligned}$$

where  $x \in \mathbb{R}^{n_{\text{eq}}}$  is the input and the other problem data are constant within the problem family.

---

<sup>3</sup>Code for experiments is available at <https://github.com/miniyachi/SnareNet>.

**Baselines.** We compare SnareNet to three baselines:

1. DC3 [10] strictly enforces equality constraints by predicting free variables and solving dependent variables from equality constraints. The inequality constraint violation are iteratively reduced by a fixed number of gradient descent steps on the free variables.
2. HardNet [28] uses soft-epochs and strictly enforces linear constraints by (4). We compare to HardNet on NCPs.
3. HProj [26] trains in two stages, rather than end-to-end: the first stage trains a homeomorphic map and the second stage trains a soft-constraint NN. At inference time, HProj uses bisection to project onto the feasible set.

**Evaluation.** Table 1 summarizes the six evaluation metrics in our experiments. Figures 4 to 5 presented below follow the same 2-by-3 layout. All experiments are run for 5 random seeds and the metrics are averaged over the seeds. The optimality gap is assessed relative to Gurobi [16]. The complete test results for the experiments in this section are provided in Section D.

	<b>Optimality Gap</b>	<b>Inequality Violation</b>	<b>Equality Violation</b>
<b>Geometric Mean</b>	$\text{gmean}_{x \in \mathcal{X}_{\text{test}}}(f_x(\hat{y}) - f_x^*)$	$\text{gmean}_{x \in \mathcal{X}_{\text{test}}} \text{gmean}_{j \in [n_{\text{ineq}}]} (j\text{-th inequality/equality violation})$	
<b>Maximum</b>	$\max_{x \in \mathcal{X}_{\text{test}}}(f_x(\hat{y}) - f_x^*)$	$\max_{x \in \mathcal{X}_{\text{test}}} \max_{j \in [n_{\text{ineq}}]} (j\text{-th inequality/equality violation})$	

Table 1: Six evaluation metrics and their layout. The function  $\text{gmean}(\cdot)$  denotes the geometric mean over a set of numbers.

**Feasibility Control and Low Variation along Training.** Figure 4 shows training dynamics for end-to-end training methods (i.e., exclude HProj) on 833 validation instances of NCPs and QCQPs. HardNet exhibits larger seed-to-seed variability in optimality gap, while DC3 shows large variability in inequality-constraint violation. In contrast, SnareNet is robust across random seeds after adaptive relaxation completes (at epoch 500, marked by vertical red dashed line). Earlier, variable violations are expected since SnareNet enforces relaxed constraints while the figures show violation of original constraints. Moreover, SnareNet successfully controls feasibility up to the specified tolerance.

**Better Optimality.** Figure 5 evaluates trained neural solvers on a separate test set for NCPs and QCQPs. SnareNet achieves optimality gaps at least one order of magnitude smaller than baseline methods while maintaining feasibility within the prescribed tolerance `tol`. HProj exhibits substantial variation in optimality gap across random seeds because its projection step is applied post-training and is not integrated into the learning objective, which can degrade optimality.

**$\lambda$  Improves Optimality Even for Linear Constraints.** SnareNet specializes to HardNet when  $\lambda = 0$  and adaptive relaxation is replaced by soft epochs for training. Setting  $\lambda > 0$  requires more than one iteration to enforce feasibility but can improve the optimality gap by orders of magnitude. See Figure 6.

**SnareNet Handles Many Constraints.** HardNet requires the linear constraint matrix  $A$  to have full row rank and is thus limited to at most  $2n$  constraints, where  $n$  is the output dimension. SnareNet overcomes this limitation through LM-regularization. Figure 7 presents test results on QCQPs with  $n = 100$  variables,  $n_{\text{eq}} = 50$  equality constraints, and  $n_{\text{ineq}} \in \{10, 50, 100\}$  inequality constraints. SnareNet consistently produces feasible solutions within tolerance  $10^{-4}$  across all test instances. In contrast, DC3 achieves feasibility on only 80% of test instances on average and exhibits

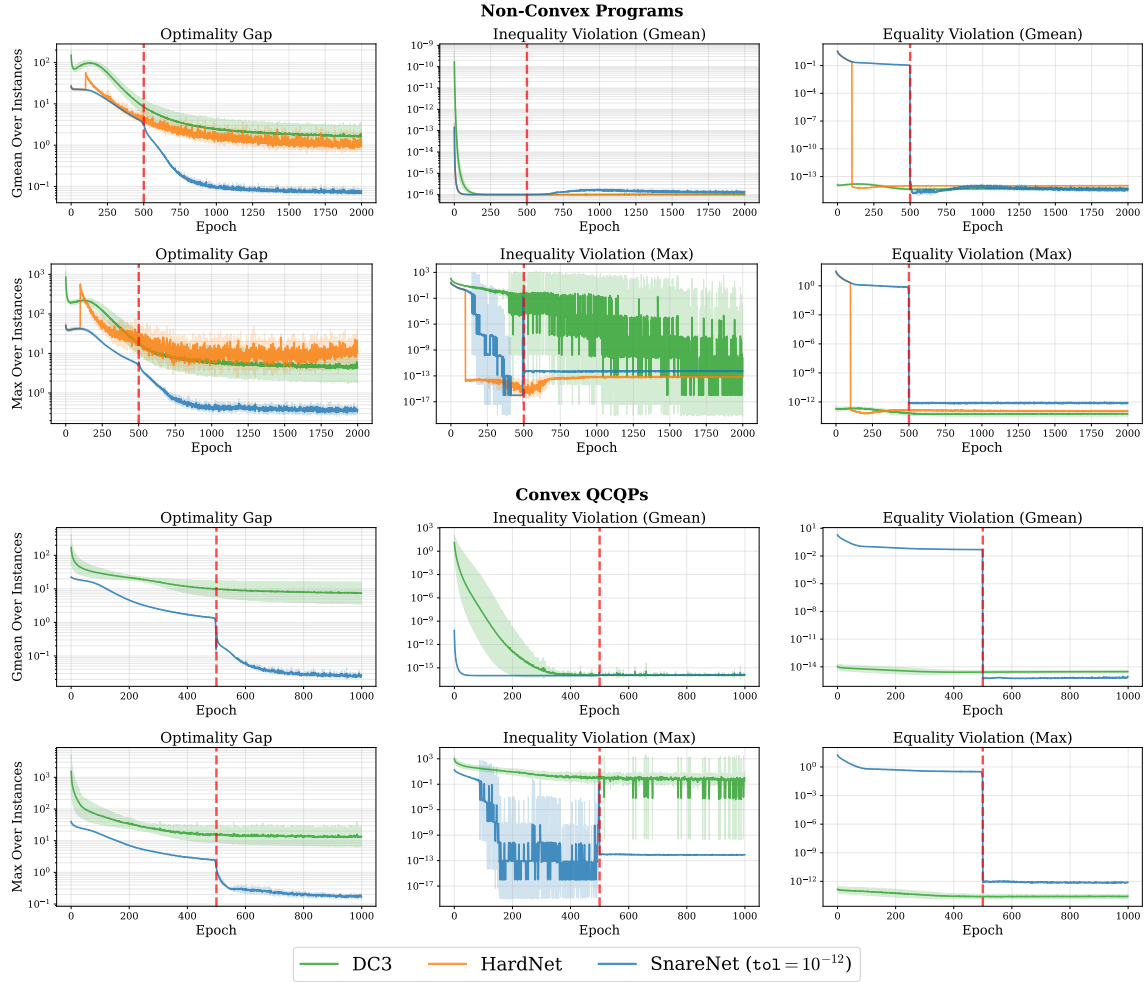


Figure 4: Training dynamics on 833 validation instances of NCPs and QCQPs. Shaded region indicate the standard deviation across seeds.

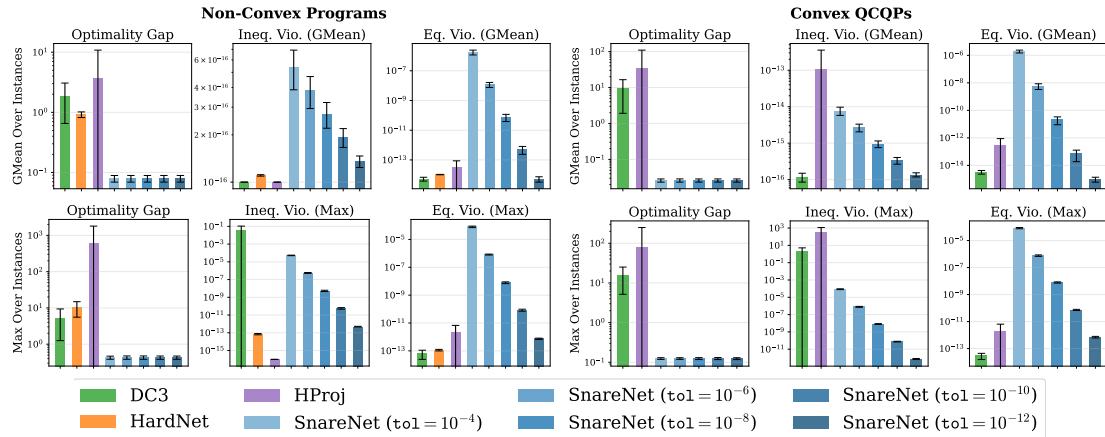


Figure 5: Evaluation metrics on 833 test instances of NCPs and QCQPs. Black error bars indicate the standard deviation across seeds.

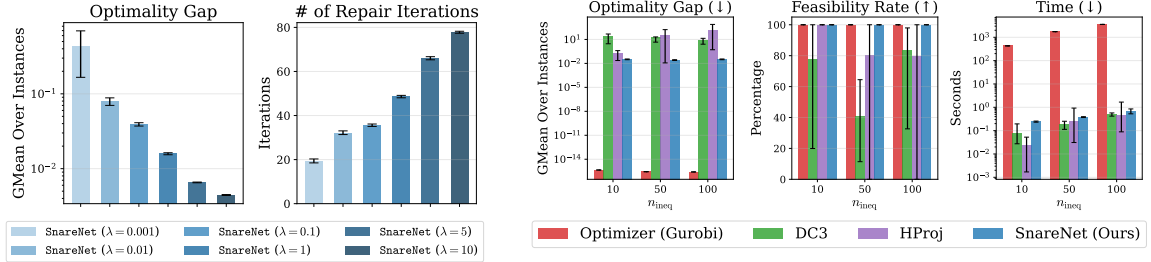


Figure 6: Optimality gap and repair iterations on 833 test instances of NCPs. Bars represent the mean across 5 random seeds, and black error bars indicate the standard deviation across seeds.

Figure 7: Performance comparison across methods for QCQPs with various number of inequality constraints. Bars represent the mean across 5 random seeds, and black error bars indicate the minimum and maximum values.

high sensitivity to random initialization. HProj shows substantial variation in feasibility rates for problems with  $n_{\text{ineq}} = 50$  and 100 inequality constraints. Inference time for the classical solver Gurobi is significantly slower than neural solvers and scales rapidly with the number of inequality constraints.

## 5.2 Neural Control Policies

Neural control policies use deep neural networks to learn mappings from system states  $x$  to control actions  $u$ , either as standalone policies or to enhance traditional control methods. In this experiment, we train a neural network policy  $\pi_\theta(x)$  to control a unicycle system, avoiding obstacle collisions by enforcing safety constraints [28, 35]. The neural policy is constructed as the sum of a nominal controller  $\pi_{\text{nom}}(x)$ , designed without obstacle awareness, and a learned correction term  $\mathcal{M}_\theta(x)$ :

$$\pi_\theta(x) := \pi_{\text{nom}}(x) + \mathcal{M}_\theta(x).$$

The system state is  $x(t) = (p_x(t), p_y(t), \theta(t), v(t), w(t)) \in \mathbb{R}^5$  at time  $t$ , where  $p_x, p_y$  are the coordinates,  $\theta$  is the heading angle,  $v$  is the linear velocity, and  $w$  is the angular velocity. The control  $u(t) = (a(t), \alpha(t)) \in \mathbb{R}^2$  includes linear acceleration  $a$  and angular acceleration  $\alpha$ . The control changes the system state by the linear dynamics:  $\dot{x} = F(x) + Gu$ , where  $F: \mathbb{R}^5 \rightarrow \mathbb{R}^5$  and  $G \in \mathbb{R}^{5 \times 2}$  are defined in Section C. Our neural policy is trained by minimizing a quadratic cost over a finite time horizon:

$$\Delta t \sum_{i=0}^{n_t} x(t_i)^T Q x(t_i) + c \|\pi_\theta(x(t_i))\|^2,$$

where  $Q = \text{diag}(100, 100, 0, 0.1, 0.1)$  penalizes deviations from the target position  $(0, 0)$  and velocity,  $c = 0.1$  weights the control effort, and  $n_t = 10$  steps for trajectories.

We use *control barrier functions* (CBFs) [2], denoted by  $h$ , to parametrize the safe set:  $h(x) \geq 0$  indicates  $x$  is a safe state. Each obstacle is represented by a distinct CBF. See Section C for CBFs used in experiment. Collision-free trajectories are guaranteed by enforcing

$$\nabla h_j(x)^T (F(x) + G\pi_\theta(x)) \geq -\alpha h_j(x) \quad (12)$$

for each obstacle with CBF  $h_j$  and some  $\alpha > 0$ . The number of constraints scales linearly with the number of obstacles. HardNet can avoid at most two obstacles as it requires full row rank constraints and the system has only two controls, whereas SnareNet handles arbitrarily many obstacles.

For training, we uniformly sample initial states with positions  $(p_x, p_y) \in [-12, 2] \times [-2, 10]$ , heading angles  $\theta \in [-\frac{\pi}{4}, -\frac{\pi}{8}]$ , and zero velocities ( $v = w = 0$ ). At inference time, we execute the learned policy for 65, 75, and 150 time steps for DC3, SnareNet, and nominal control, respectively. Results appear in Figure 8.

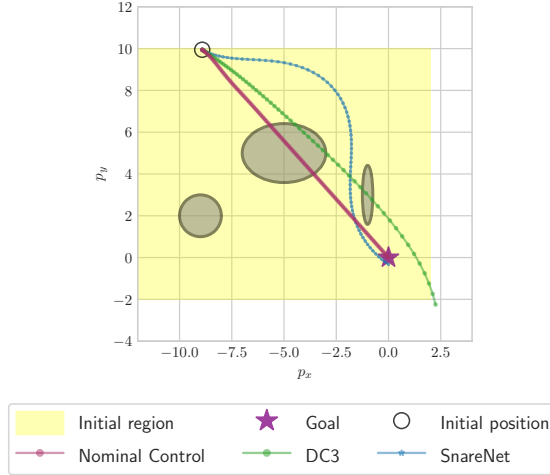


Figure 8: Simulated unicycle trajectories from a random starting point inside the initialization region.

## 6 Conclusion

We introduce SnareNet, a practical framework to enforce nonlinear input-dependent constraints in NNs. Our key innovations include regularization for stable optimization, Newton updates for efficient convergence, explicit infeasibility tolerances for controllable constraint enforcement, and adaptive relaxation that progressively tightens the constraints. Our empirical evaluation demonstrates that SnareNet consistently produces feasible solutions with better objective values across optimization learning tasks and neural control policies. An important direction for future work is to understand how hard constraints, relaxed constraints, and soft constraints fundamentally alter the learnability of deep neural networks.

## References

- [1] Aaron D Ames, Xiangru Xu, Jessy W Grizzle, and Paulo Tabuada. Control barrier function based quadratic programs for safety critical systems. *IEEE Transactions on Automatic Control*, 62(8):3861–3876, 2016.
- [2] Aaron D. Ames, Samuel Coogan, Magnus Egerstedt, Gennaro Notomista, Koushil Sreenath, and Paulo Tabuada. Control barrier functions: Theory and applications, 2019. URL <https://arxiv.org/abs/1903.11199>.
- [3] Brandon Amos and J Zico Kolter. Optnet: Differentiable optimization as a layer in neural networks. In *International conference on machine learning*, pages 136–145. PMLR, 2017.
- [4] Christof Angermueller, Tanel Pärnamaa, Leopold Parts, and Oliver Stegle. Deep learning for computational biology. *Molecular systems biology*, 12(7):878, 2016.
- [5] Tom Beucler, Michael Pritchard, Stephan Rasp, Jordan Ott, Pierre Baldi, and Pierre Gentine. Enforcing analytic constraints in neural networks emulating physical systems. *Physical Review Letters*, 126(9), March 2021. ISSN 1079-7114. doi: 10.1103/physrevlett.126.098302. URL <http://dx.doi.org/10.1103/PhysRevLett.126.098302>.
- [6] Boris Bonev, Thorsten Kurth, Ankur Mahesh, Mauro Bisson, Jean Kossaifi, Karthik Kashinath, Anima Anandkumar, William D Collins, Michael S Pritchard, and Alexander Keller. Fourcastnet

3: A geometric approach to probabilistic machine-learning weather forecasting at scale. *arXiv preprint arXiv:2507.12144*, 2025.

[7] Hao Chen, Gonzalo E. Constante Flores, and Can Li. Physics-informed neural networks with hard linear equality constraints, 2024. URL <https://arxiv.org/abs/2402.07251>.

[8] Siyuan Chen, Minghao Guo, Caoliwen Wang, Anka He Chen, Yikun Zhang, Jingjing Chai, Yin Yang, Wojciech Matusik, and Peter Yichen Chen. Physically valid biomolecular interaction modeling with gauss-seidel projection. *arXiv preprint arXiv:2510.08946*, 2025.

[9] Alp Dener, Marco Andres Miller, Randy Michael Churchill, Todd Munson, and Choong-Seock Chang. Training neural networks under physical constraints using a stochastic augmented lagrangian approach, 2020. URL <https://arxiv.org/abs/2009.07330>.

[10] Priya L Donti, David Rolnick, and J Zico Kolter. Dc3: A learning method for optimization with hard constraints. *arXiv preprint arXiv:2104.12225*, 2021.

[11] N. Benjamin Erichson, Michael Muehlebach, and Michael W. Mahoney. Physics-informed autoencoders for lyapunov-stable fluid flow prediction, 2019. URL <https://arxiv.org/abs/1905.10866>.

[12] Thomas Frerix, Matthias Nießner, and Daniel Cremers. Homogeneous linear inequality constraints for neural network activations, 2020. URL <https://arxiv.org/abs/1902.01785>.

[13] Rafael Gómez-Bombarelli, Jennifer N Wei, David Duvenaud, José Miguel Hernández-Lobato, Benjamín Sánchez-Lengeling, Dennis Sheberla, Jorge Aguilera-Iparraguirre, Timothy D Hirzel, Ryan P Adams, and Alán Aspuru-Guzik. Automatic chemical design using a data-driven continuous representation of molecules. *ACS central science*, 4(2):268–276, 2018.

[14] Sorin Grigorescu, Bogdan Trasnea, Tiberiu Cocias, and Gigel Macesanu. A survey of deep learning techniques for autonomous driving. *Journal of field robotics*, 37(3):362–386, 2020.

[15] Panagiotis D Grontas, Antonio Terpin, Efe C Balta, Raffaello D’Andrea, and John Lygeros. Pinet: Optimizing hard-constrained neural networks with orthogonal projection layers. *arXiv preprint arXiv:2508.10480*, 2025.

[16] Gurobi Optimization, LLC. Gurobi Optimizer Reference Manual, 2024. URL <https://www.gurobi.com>.

[17] Ashfaq Iftakher, Rahul Golder, Bimol Nath Roy, and MM Faruque Hasan. Physics-informed neural networks with hard nonlinear equality and inequality constraints. *Computers & Chemical Engineering*, page 109418, 2025.

[18] John Jumper, Richard Evans, Alexander Pritzel, Tim Green, Michael Figurnov, Olaf Ronneberger, Kathryn Tunyasuvunakool, Russ Bates, Augustin Žídek, Anna Potapenko, et al. Highly accurate protein structure prediction with alphafold. *nature*, 596(7873):583–589, 2021.

[19] Hoel Kervadec, Jose Dolz, Meng Tang, Eric Granger, Yuri Boykov, and Ismail Ben Ayed. Constrained-cnn losses for weakly supervised segmentation. *Medical Image Analysis*, 54:88–99, May 2019. ISSN 1361-8415. doi: 10.1016/j.media.2019.02.009. URL <http://dx.doi.org/10.1016/j.media.2019.02.009>.

[20] Hoel Kervadec, Jose Dolz, Jing Yuan, Christian Desrosiers, Eric Granger, and Ismail Ben Ayed. Constrained deep networks: Lagrangian optimization via log-barrier extensions. In *2022 30th European Signal Processing Conference (EUSIPCO)*, page 962–966. IEEE, August 2022. doi: 10.23919/eusipco55093.2022.9909927. URL <http://dx.doi.org/10.23919/EUSIPCO55093.2022.9909927>.

[21] Dmitrii Kochkov, Jamie A Smith, Ayya Alieva, Qing Wang, Michael P Brenner, and Stephan Hoyer. Machine learning-accelerated computational fluid dynamics. *Proceedings of the National Academy of Sciences*, 118(21):e2101784118, 2021.

[22] Remi Lam, Alvaro Sanchez-Gonzalez, Matthew Willson, Peter Wirnsberger, Meire Fortunato, Ferran Alet, Suman Ravuri, Timo Ewalds, Zach Eaton-Rosen, Weihua Hu, et al. Learning skillful medium-range global weather forecasting. *Science*, 382(6677):1416–1421, 2023.

[23] Sergey Levine, Chelsea Finn, Trevor Darrell, and Pieter Abbeel. End-to-end training of deep visuomotor policies. *Journal of Machine Learning Research*, 17(39):1–40, 2016.

[24] Meiyi Li, Soheil Kolouri, and Javad Mohammadi. Learning to solve optimization problems with hard linear constraints. *IEEE Access*, 11:59995–60004, 2023.

[25] Zongyi Li, Hongkai Zheng, Nikola Kovachki, David Jin, Haoxuan Chen, Burigede Liu, Kamyar Azizzadenesheli, and Anima Anandkumar. Physics-informed neural operator for learning partial differential equations. *ACM/IMS Journal of Data Science*, 1(3):1–27, 2024.

[26] Enming Liang, Minghua Chen, and Steven H. Low. Homeomorphic projection to ensure neural-network solution feasibility for constrained optimization. *Journal of Machine Learning Research*, 25(329):1–55, 2024. URL <http://jmlr.org/papers/v25/23-1577.html>.

[27] Lu Lu, Raphael Pestourie, Wenjie Yao, Zhicheng Wang, Francesc Verdugo, and Steven G Johnson. Physics-informed neural networks with hard constraints for inverse design. *SIAM Journal on Scientific Computing*, 43(6):B1105–B1132, 2021.

[28] Youngjae Min and Navid Azizan. Hardnet: Hard-constrained neural networks with universal approximation guarantees. *arXiv preprint arXiv:2410.10807*, 2024.

[29] Pablo Márquez-Neila, Mathieu Salzmann, and Pascal Fua. Imposing hard constraints on deep networks: Promises and limitations, 2017. URL <https://arxiv.org/abs/1706.02025>.

[30] Hoang T Nguyen and Priya L Donti. Fsnet: Feasibility-seeking neural network for constrained optimization with guarantees. *arXiv preprint arXiv:2506.00362*, 2025.

[31] Xiang Pan. Deepopf: deep neural networks for optimal power flow. In *Proceedings of the 8th ACM International Conference on Systems for Energy-Efficient Buildings, Cities, and Transportation*, pages 250–251, 2021.

[32] John Platt and Alan Barr. Constrained differential optimization. In *Neural information processing systems*, 1987.

[33] Maziar Raissi, Paris Perdikaris, and George E Karniadakis. Physics-informed neural networks: A deep learning framework for solving forward and inverse problems involving nonlinear partial differential equations. *Journal of Computational physics*, 378:686–707, 2019.

[34] Pratik Rathore, Weimu Lei, Zachary Frangella, Lu Lu, and Madeleine Udell. Challenges in training pinns: A loss landscape perspective. *arXiv preprint arXiv:2402.01868*, 2024.

[35] Manan Tayal, Bhavya Giri Goswami, Karthik Rajgopal, Rajpal Singh, Tejas Rao, Jishnu Keshavan, Pushpak Jagtap, and Shishir Kolathaya. A collision cone approach for control barrier functions, 2024. URL <https://arxiv.org/abs/2403.07043>.

[36] Jesus Tordesillas, Jonathan P. How, and Marco Hutter. Rayen: Imposition of hard convex constraints on neural networks, 2023. URL <https://arxiv.org/abs/2307.08336>.

[37] Pascal Van Hentenryck. Optimization learning. *arXiv preprint arXiv:2501.03443*, 2025.

- [38] Grady Williams, Nolan Wagener, Brian Goldfain, Paul Drews, James M Rehg, Byron Boots, and Evangelos A Theodorou. Information theoretic mpc for model-based reinforcement learning. In *2017 IEEE international conference on robotics and automation (ICRA)*, pages 1714–1721. IEEE, 2017.
- [39] Zhenqin Wu, Bharath Ramsundar, Evan N Feinberg, Joseph Gomes, Caleb Geniesse, Aneesh S Pappu, Karl Leswing, and Vijay Pande. Moleculenet: a benchmark for molecular machine learning. *Chemical science*, 9(2):513–530, 2018.
- [40] Jingyi Xu, Zilu Zhang, Tal Friedman, Yitao Liang, and Guy Van den Broeck. A semantic loss function for deep learning with symbolic knowledge, 2018. URL <https://arxiv.org/abs/1711.11157>.
- [41] Shengwei Zhang and AG Constantinides. Lagrange programming neural networks. *IEEE Transactions on Circuits and Systems II: Analog and Digital Signal Processing*, 39(7):441–452, 1992.

## A Related Literature

**Penalty Methods.** Early approaches to enforcing constraints in neural networks add penalty terms to the loss function [29]. These methods augment the original objective with a term that penalizes constraint violations, also called a *soft loss*, allowing the use of standard unconstrained optimization techniques during training. Due to the use of a soft loss, methods using the penalty formulation are also called soft-constrained methods in related works [28, 15]. This methodology is commonly used for data-parameterized constrained optimization problems [37] and for solving partial differential equations [33, 9, 11, 27]. Another application of penalty methods is for convolutional neural networks to perform weakly supervised medical image segmentation [19, 20]. Xu et al. [40] also uses a soft loss to encourage the neural network’s output probabilities to satisfy a propositional logic formula.

**Hard-Constraint Methods.** An alternative approach seeks to impose constraints on the solutions by modifying the neural network outputs to be feasible by construction. One early architecture parameterizes the feasible set for homogeneous linear constraints and embeds it in the neural network’s activation functions [12]. Multiple methods, such as KKT-hPINNs [7] and KKT-HardNet [17], leverage the KKT conditions to enforce both hard equality and inequality constraints. RAYEN enforces hard convex input-independent constraints by interpolating between the neural network output and an interior point of the feasible set [36]. Beucler et al. [5] enforces hard nonlinear constraints by linearizing the constraints, learning a subset of independent variables, and performing equality completion to determine the dependent variables. DC3 predicts an initial solution using a soft penalty formulation and moves it toward the feasible region via equality completion and gradient descent on the distance to feasibility [10]. IInet decomposes an affine feasible set as the intersection of two higher-dimensional convex sets and applies Douglas-Rachford algorithm to find a feasible solution, in which the computational efficiency is improved by restricting the framework to linear and box constraints [15]. HardNet [28] uses a closed-form repair layer that guarantees exact linear feasibility up to machine precision and enables efficient backpropagation. Li et al. [24] uses a learned gauge function to map the  $\ell_\infty$  unit ball to the feasible set for linear constraints. Similarly, Homeomorphic Projection [26] constrains solutions onto a convex (and certain non-convex) domain by learning a homeomorphic mapping from the feasible set to the unit ball, projecting the solution, and applying the inverse mapping.

---

**Algorithm 2** Training paradigm of SnareNet

---

```

1: function TRAIN( $\mathcal{X}_{\text{train}}$ )
2:   init neural network  $\mathcal{M}_\theta : \mathbb{R}^d \rightarrow \mathbb{R}^n$  and  $\lambda \geq 0$ 
3:   init constraint violation  $\varepsilon_x^{(0)}$  for  $x \in \mathcal{X}_{\text{train}}$ 
4:   set a relaxation parameter schedule  $\{\varepsilon_x^{(t)}\}_{t=1}^T$ 
5:   for epoch  $t = 1, 2, \dots, T$  do
6:     for mini-batch  $\mathcal{B} \subset \mathcal{X}_{\text{train}}$  do
7:       compute approximate solution  $\hat{y}_i = \mathcal{M}_\theta(x_i)$  for all  $x_i \in \mathcal{B}$ 
8:       repair to relaxed feasible solution  $\check{y}_i = \mathcal{R}(\hat{y}_i, \lambda, \varepsilon_x^{(t)})$  for all  $x_i \in \mathcal{B}$ 
9:       compute batch loss  $\mathcal{L}_{\mathcal{B}}(\theta)$ 
10:      update  $\theta$  using  $\nabla_\theta \mathcal{L}_{\mathcal{B}}(\theta)$ 
11:    end for
12:  end for
13: end function

```

---

## B Training Algorithm of SnareNet

Algorithm 2 provides the complete pseudocode for SnareNet’s training algorithm.

## C Neural Control Policies Experiment Details

The unicycle system follows the linear dynamics  $\dot{x} = F(x) + Gu$ , where

$$F(x) = \begin{bmatrix} v \cos \theta \\ v \sin \theta \\ w \\ 0 \\ 0 \end{bmatrix} \quad \text{and} \quad G(x) = \begin{bmatrix} 0 & 0 \\ 0 & 0 \\ 0 & 0 \\ 1 & 0 \\ 0 & 1 \end{bmatrix}.$$

For an elliptical obstacle centered at  $(c_x, c_y)$  with axes  $(r_x, r_y)$ , we use the higher order CBF  $h(x) = \dot{h}_e(x) + \kappa h_e(x)$  with  $\kappa > 0$ , [28] in our experiments, where

$$h_e(x) = \left( \frac{c_x - p_x + \ell \cos \theta}{r_x} \right)^2 + \left( \frac{c_y - p_y + \ell \sin \theta}{r_y} \right)^2 - 1.$$

## D Tables for All Test Results in Section 5.1

This section includes all the evaluation results on test instances for experiments in Section 5.1. For ease of navigation, Table 2 summarizes the correspondence between figures presented in the main text and their associated results tables organized by problem class. Columns “# of Ineq. Violations” and “# of Eq. Violations” are counted with threshold  $10^{-4}$ .

Tables	Problem Class	Figures
Table 3	NCP	Figure 4 & Figure 5
Table 4	QCQP	Figure 4 & Figure 5
Table 5	NCP	Figure 6
Table 6	QCQP (10 inequality constraints)	Figure 7
Table 7	QCQP (50 inequality constraints)	Figure 7
Table 8	QCQP (100 inequality constraints)	Figure 7

Table 2: Correspondence between tables, problem classes, and figures in main paper.

Table 3: Evaluation metrics on the NCP test set. Values shown as mean  $\pm$  std across 5 random seeds.

Method	Max Opt. Gap	GMean Opt. Gap	GMean Ineq. Error	# Ineq Violations	Max Eq. Error	GMean Eq. Error	# Eq Violations	Test Time (s)
DC3	5.31 $\pm$ 4.05	1.86 $\pm$ 1.21	(1.00 $\pm$ 0.00) $\times 10^{-16}$	(7.20 $\pm$ 10.74) $\times 10^{-4}$	(6.76 $\pm$ 4.32) $\times 10^{-14}$	(5.29 $\pm$ 1.54) $\times 10^{-15}$	0.00	0.14 $\pm$ 0.10
HardNet	(1.02 $\pm$ 0.47) $\times 10^1$	(9.17 $\pm$ 0.99) $\times 10^{-1}$	(1.10 $\pm$ 0.01) $\times 10^{-13}$	0.00	(1.13 $\pm$ 0.14) $\times 10^{-13}$	(1.04 $\pm$ 0.03) $\times 10^{-14}$	0.00	0.05 $\pm$ 0.01
HProj	(5.97 $\pm$ 12.04) $\times 10^2$	3.72 $\pm$ 7.12	0.00	0.00	(2.24 $\pm$ 4.49) $\times 10^{-13}$	(3.12 $\pm$ 5.58) $\times 10^{-14}$	0.00	0.05 $\pm$ 0.03
SnareNet (tol = 10 <sup>-12</sup> )	(4.26 $\pm$ 0.44) $\times 10^{-1}$	(7.91 $\pm$ 1.00) $\times 10^{-2}$	(1.35 $\pm$ 0.11) $\times 10^{-16}$	0.00	(7.34 $\pm$ 0.83) $\times 10^{-13}$	(5.27 $\pm$ 2.07) $\times 10^{-15}$	0.00	0.80 $\pm$ 0.14
SnareNet (tol = 10 <sup>-4</sup> )	(4.26 $\pm$ 0.42) $\times 10^{-1}$	(7.90 $\pm$ 1.00) $\times 10^{-2}$	(5.40 $\pm$ 0.53) $\times 10^{-16}$	0.00	(8.07 $\pm$ 1.00) $\times 10^{-5}$	(1.81 $\pm$ 6.64) $\times 10^{-6}$	0.00	0.33 $\pm$ 0.05
SnareNet (tol = 10 <sup>-6</sup> )	(4.28 $\pm$ 0.45) $\times 10^{-1}$	(7.90 $\pm$ 1.01) $\times 10^{-2}$	(3.82 $\pm$ 0.88) $\times 10^{-16}$	0.00	(8.24 $\pm$ 0.64) $\times 10^{-7}$	(1.20 $\pm$ 0.44) $\times 10^{-8}$	0.00	0.46 $\pm$ 0.17
SnareNet (tol = 10 <sup>-8</sup> )	(4.28 $\pm$ 0.46) $\times 10^{-1}$	(7.90 $\pm$ 1.00) $\times 10^{-2}$	(2.71 $\pm$ 0.51) $\times 10^{-16}$	0.00	(7.88 $\pm$ 1.14) $\times 10^{-9}$	(7.74 $\pm$ 3.91) $\times 10^{-11}$	0.00	0.64 $\pm$ 0.26
SnareNet (tol = 10 <sup>-10</sup> )	(4.26 $\pm$ 0.45) $\times 10^{-1}$	(7.91 $\pm$ 1.00) $\times 10^{-2}$	(1.93 $\pm$ 0.26) $\times 10^{-16}$	0.00	(8.42 $\pm$ 1.36) $\times 10^{-11}$	(5.23 $\pm$ 2.86) $\times 10^{-13}$	0.00	0.88 $\pm$ 0.18

Table 4: Evaluation metrics on the QCQP test set. Values shown as mean  $\pm$  std across 5 random seeds.

Method	Max Opt. Gap	GMean Opt. Gap	GMean Ineq. Error	# Ineq Violations	Max Eq. Error	GMean Eq. Error	# Eq Violations	Test Time (s)
DC3	(1.52 $\pm$ 1.00) $\times 10^1$	9.22 $\pm$ 7.30	(1.17 $\pm$ 0.32) $\times 10^{-16}$	0.19 $\pm$ 0.33	(3.00 $\pm$ 1.45) $\times 10^{-14}$	(3.28 $\pm$ 0.98) $\times 10^{-15}$	0.00	0.15 $\pm$ 0.06
HProj	(7.78 $\pm$ 17.18) $\times 10^1$	(3.41 $\pm$ 7.57) $\times 10^1$	(1.10 $\pm$ 2.47) $\times 10^{-13}$	10.00 $\pm$ 22.36	(2.01 $\pm$ 4.41) $\times 10^{-12}$	(2.77 $\pm$ 6.08) $\times 10^{-13}$	0.00	0.26 $\pm$ 0.37
SnareNet (tol = 10 <sup>-12</sup> )	(1.24 $\pm$ 0.06) $\times 10^{-1}$	(2.60 $\pm$ 0.26) $\times 10^{-2}$	(1.36 $\pm$ 0.17) $\times 10^{-16}$	0.00	(7.06 $\pm$ 0.95) $\times 10^{-13}$	(9.93 $\pm$ 3.87) $\times 10^{-16}$	0.00	1.37 $\pm$ 0.48
SnareNet (tol = 10 <sup>-4</sup> )	(1.24 $\pm$ 0.06) $\times 10^{-1}$	(2.60 $\pm$ 0.26) $\times 10^{-2}$	(7.74 $\pm$ 1.97) $\times 10^{-15}$	0.00	(8.33 $\pm$ 0.87) $\times 10^{-5}$	(1.93 $\pm$ 0.45) $\times 10^{-6}$	0.00	0.69 $\pm$ 0.74
SnareNet (tol = 10 <sup>-6</sup> )	(1.25 $\pm$ 0.06) $\times 10^{-1}$	(2.60 $\pm$ 0.27) $\times 10^{-2}$	(2.68 $\pm$ 0.64) $\times 10^{-15}$	0.00	(7.64 $\pm$ 0.97) $\times 10^{-7}$	(5.92 $\pm$ 2.64) $\times 10^{-9}$	0.00	0.79 $\pm$ 0.28
SnareNet (tol = 10 <sup>-8</sup> )	(1.24 $\pm$ 0.07) $\times 10^{-1}$	(2.60 $\pm$ 0.26) $\times 10^{-2}$	(9.52 $\pm$ 1.98) $\times 10^{-16}$	0.00	(7.88 $\pm$ 0.82) $\times 10^{-9}$	(2.13 $\pm$ 1.23) $\times 10^{-11}$	0.00	1.18 $\pm$ 0.17
SnareNet (tol = 10 <sup>-10</sup> )	(1.25 $\pm$ 0.07) $\times 10^{-1}$	(2.60 $\pm$ 0.26) $\times 10^{-2}$	(3.35 $\pm$ 0.70) $\times 10^{-16}$	0.00	(7.31 $\pm$ 0.72) $\times 10^{-11}$	(7.35 $\pm$ 5.48) $\times 10^{-14}$	0.00	1.57 $\pm$ 0.46

Table 5: Evaluation metrics on the NCP test set. Values shown as mean  $\pm$  std across 5 random seeds.

Method	Obj. Value	Max Opt. Gap	GMean Opt. Gap	Max Ineq. Error	GMean Ineq. Error	# Ineq Violations	Max Eq. Error	GMean Eq. Error	# Eq Violations	Test Time (s)
SnareNet ( $\lambda = 0.001$ )	-11.19 $\pm$ 0.29	2.92 $\pm$ 1.73	(4.28 $\pm$ 2.66) $\times 10^{-1}$	(4.07 $\pm$ 1.46) $\times 10^{-9}$	(1.72 $\pm$ 0.14) $\times 10^{-16}$	0.00	(6.57 $\pm$ 2.36) $\times 10^{-9}$	(1.87 $\pm$ 0.97) $\times 10^{-10}$	0.00	0.28 $\pm$ 0.12
SnareNet ( $\lambda = 0.01$ )	-11.59 $\pm$ 0.01	(4.28 $\pm$ 0.46) $\times 10^{-1}$	(7.90 $\pm$ 1.00) $\times 10^{-2}$	(5.35 $\pm$ 0.88) $\times 10^{-9}$	(2.71 $\pm$ 0.51) $\times 10^{-16}$	0.00	(7.88 $\pm$ 1.14) $\times 10^{-9}$	(7.74 $\pm$ 3.91) $\times 10^{-11}$	0.00	0.76 $\pm$ 0.74
SnareNet ( $\lambda = 0.1$ )	-11.64 $\pm$ 0.00	(2.18 $\pm$ 0.12) $\times 10^{-1}$	(3.86 $\pm$ 0.22) $\times 10^{-2}$	(1.40 $\pm$ 0.22) $\times 10^{-8}$	(2.58 $\pm$ 0.04) $\times 10^{-16}$	0.00	(2.08 $\pm$ 0.33) $\times 10^{-8}$	(4.29 $\pm$ 0.82) $\times 10^{-10}$	0.00	0.61 $\pm$ 0.26
SnareNet ( $\lambda = 10$ )	-11.67 $\pm$ 0.00	(1.87 $\pm$ 0.16) $\times 10^{-2}$	(4.29 $\pm$ 0.06) $\times 10^{-3}$	(8.65 $\pm$ 0.46) $\times 10^{-8}$	(6.38 $\pm$ 0.16) $\times 10^{-16}$	0.00	(1.20 $\pm$ 0.06) $\times 10^{-7}$	(4.98 $\pm$ 0.61) $\times 10^{-9}$	0.00	2.19 $\pm$ 1.24
SnareNet ( $\lambda = 1$ )	-11.66 $\pm$ 0.00	(6.99 $\pm$ 0.74) $\times 10^{-2}$	(1.57 $\pm$ 0.05) $\times 10^{-2}$	(1.96 $\pm$ 0.08) $\times 10^{-8}$	(5.01 $\pm$ 0.09) $\times 10^{-16}$	0.00	(3.21 $\pm$ 0.13) $\times 10^{-8}$	(6.27 $\pm$ 0.93) $\times 10^{-10}$	0.00	1.31 $\pm$ 0.32
SnareNet ( $\lambda = 5$ )	-11.67 $\pm$ 0.00	(2.74 $\pm$ 0.08) $\times 10^{-2}$	(6.34 $\pm$ 0.06) $\times 10^{-3}$	(5.07 $\pm$ 0.25) $\times 10^{-8}$	(6.78 $\pm$ 0.12) $\times 10^{-16}$	0.00	(7.52 $\pm$ 0.39) $\times 10^{-8}$	(3.19 $\pm$ 0.24) $\times 10^{-9}$	0.00	2.22 $\pm$ 1.17

Table 6: Evaluation metrics on the QCQP with 10 inequality constraints test set. Values shown as mean  $\pm$  std across 5 random seeds.

Method	Max Opt. Gap	GMean Opt. Gap	GMean Ineq. Error	# Ineq Violations	Max Eq. Error	GMean Eq. Error	# Eq Violations	Test Time (s)
Optimizer (Gurobi)	1.42 $\times 10^{-14}$	4.48 $\times 10^{-16}$	0.00	0.00	5.43 $\times 10^{-10}$	1.06 $\times 10^{-14}$	0.00	428.44
DC3	(7.96 $\pm$ 11.33) $\times 10^1$	(2.21 $\pm$ 1.94) $\times 10^1$	(3.52 $\pm$ 7.87) $\times 10^{-10}$	0.97 $\pm$ 1.88	(1.48 $\pm$ 1.11) $\times 10^{-13}$	(1.40 $\pm$ 0.94) $\times 10^{-14}$	0.00	0.08 $\pm$ 0.07
HProj	(2.40 $\pm$ 1.99) $\times 10^{-1}$	(1.60 $\pm$ 1.42) $\times 10^{-1}$	0.00	0.00	(1.08 $\pm$ 0.92) $\times 10^{-13}$	(1.41 $\pm$ 0.98) $\times 10^{-14}$	0.00	0.02 $\pm$ 0.02
SnareNet (Ours)	(1.74 $\pm$ 0.08) $\times 10^{-1}$	(3.16 $\pm$ 0.29) $\times 10^{-2}$	(4.78 $\pm$ 0.92) $\times 10^{-15}$	0.00	(5.13 $\pm$ 1.28) $\times 10^{-5}$	(6.35 $\pm$ 1.68) $\times 10^{-7}$	0.00	0.25 $\pm$ 0.01

Table 7: Evaluation metrics on the QCQP with 50 inequality constraints test set. Values shown as mean  $\pm$  std across 5 random seeds.

Method	Max Opt. Gap	GMean Opt. Gap	GMean Ineq. Error	# Ineq Violations	Max Eq. Error	GMean Eq. Error	# Eq Violations	Test Time (s)
Optimizer (Gurobi)	7.11 $\times 10^{-15}$	2.74 $\times 10^{-16}$	1.01 $\times 10^{-16}$	0.00	1.58 $\times 10^{-8}$	3.89 $\times 10^{-13}$	0.00	1742.79
DC3	(3.37 $\pm$ 1.78) $\times 10^1$	(1.59 $\pm$ 0.76) $\times 10^1$	(2.39 $\pm$ 4.72) $\times 10^{-13}$	5.33 $\pm$ 5.07	(7.63 $\pm$ 5.12) $\times 10^{-14}$	(5.42 $\pm$ 3.01) $\times 10^{-15}$	0.00	0.18 $\pm$ 0.08
HProj	(7.78 $\pm$ 17.18) $\times 10^1$	(3.41 $\pm$ 7.57) $\times 10^1$	(1.10 $\pm$ 2.47) $\times 10^{-13}$	10.00 $\pm$ 22.36	(2.01 $\pm$ 4.41) $\times 10^{-12}$	(2.77 $\pm$ 6.08) $\times 10^{-13}$	0.00	0.26 $\pm$ 0.37
SnareNet (Ours)	(1.25 $\pm$ 0.06) $\times 10^{-1}$	(2.60 $\pm$ 0.27) $\times 10^{-2}$	(2.68 $\pm$ 0.64) $\times 10^{-15}$	0.00	(7.64 $\pm$ 0.97) $\times 10^{-7}$	(5.92 $\pm$ 2.64) $\times 10^{-9}$	0.00	0.39 $\pm$ 0.01

Table 8: Evaluation metrics on the QCQP with 100 inequality constraints test set. Values shown as mean  $\pm$  std across 5 random seeds.

Method	Max Opt. Gap	GMean Opt. Gap	GMean Ineq. Error	# Ineq Violations	Max Eq. Error	GMean Eq. Error	# Eq Violations	Test Time (s)
Optimizer (Gurobi)	7.11 $\times 10^{-15}$	2.57 $\times 10^{-16}$	1.04 $\times 10^{-16}$	0.00	1.57 $\times 10^{-7}$	7.90 $\times 10^{-13}$	0.00	3563.30
DC3	(1.14 $\pm$ 0.66) $\times 10^1$	6.86 $\pm$ 4.63	(1.42 $\pm$ 0.91) $\times 10^{-16}$	0.65 $\pm$ 1.37	(1.76 $\pm$ 1.27) $\times 10^{-14}$	(1.70 $\pm$ 0.89) $\times 10^{-15}$	0.00	0.48 $\pm$ 0.08
HProj	(2.35 $\pm$ 5.22) $\times 10^2$	(1.53 $\pm$ 3.40) $\times 10^2$	(5.40 $\pm$ 12.08) $\times 10^{-11}$	20.07 $\pm$ 44.86	(1.83 $\pm$ 4.03) $\times 10^{-12}$	(3.04 $\pm$ 6.73) $\times 10^{-13}$	0.00	0.44 $\pm$ 0.69
SnareNet (Ours)	(1.74 $\pm$ 0.08) $\times 10^{-1}$	(3.16 $\pm$ 0.29) $\times 10^{-2}$	(1.88 $\pm$ 0.22) $\times 10^{-15}$	0.00	(7.77 $\pm$ 0.54) $\times 10^{-7}$	(2.80 $\pm$ 0.97) $\times 10^{-9}$	0.00	0.68 $\pm$ 0.12